Enhanced Dry Reforming of Methane on Ni and Ni-Pt Catalysts Synthesized by Atomic Layer Deposition

Troy D. Gould, Matthew M. Montemore, Alia M. Lubers, Lucas D. Ellis, Alan W. Weimer, John L. Falconer, J. Will Medlin*

University of Colorado Boulder, Department of Chemical and Biological Engineering, 3415 Colorado Ave. Boulder, CO 80303

*Will.Medlin@colorado.edu, tel: 303-492-2418, fax: 303-492-4341

Keywords: atomic layer deposition, dry reforming of methane, bimetallic catalysts, density functional theory

ABSTRACT: Atomic layer deposition (ALD) was used to deposit Ni and Pt on alumina supports to form monometallic and bimetallic catalysts with initial particle sizes of 1 to 2.4 nm. The ALD catalysts were more active (per mass of metal) than catalysts prepared by incipient wetness (IW) for dry reforming of methane (DRM), and they did not form carbon whiskers during reaction due to their sufficiently small size. Catalysts modified by Pt ALD had higher rates of reaction per mass of metal and inhibited coking, whereas NiPt catalysts synthesized by IW still formed carbon whiskers. Temperature-programmed reduction of Ni catalysts modified by Pt ALD indicated the presence of bimetallic interaction. Density functional theory calculations suggested that under reaction conditions, the NiPt surfaces form Ni-terminated surfaces that are associated with higher DRM rates (due to their C and O adsorption energies, as well as the CO formation and CH_4 dissociation energies).

1. Introduction

Recent advances in natural gas recovery and the associated drop in price of natural gas have drawn much attention to methane steam reforming and dry reforming of methane (DRM) with CO_2. Increases in global demand for transportation grade fuels and efforts to cap the amount of gas released or burned in blowouts have made gas to liquids (GTL) technologies more attractive.[1] The most widely used and economically viable GTL process is Fischer-Tropsch (F-T), which requires a syngas feed stream that is produced mainly by methane reforming.[1, 2] Nickel, which is the primary catalyst used for these reforming reactions, is plagued by deactivation due to sintering and coking.[3, 4] Sintering decreases the metal surface area, and coking can build up enough carbon to clog or alter flow in reactors, cause overheating in tubular reformers, and destroy catalyst particles.[3, 5] The carbon whiskers formed during coking do not strongly affect the reforming rate initially because the carbon diffuses from the Ni active surface to the rear of the particle where the carbon whisker is attached.[3, 6] Reforming reactions are typically run at 700 to 800°C to thermodynamically limit the reverse water-gas shift (RWGS) side reaction and coking from the Boudouard reaction, but these high temperatures exacerbate sintering and are energy-intensive.[7] Promoters, such as K and Au, limit coking by acting as step-edge site blockers or by decreasing the carbon adsorption energy to prevent carbon nucleation on the catalyst.[5, 8] A recent density functional theory (DFT) study on graphite formation from CH_4 decomposition indicated that carbon preferentially nucleates on Ni(211) step edges as opposed to terrace sites.[5] This study also calculated that a Ni step edge must be longer than 2.5 nm to form a stable carbon cluster from which more carbon can grow.

Several studies have shown that adding Pt to Ni catalysts improves DRM activity and stability at temperatures of 500 to 700°C.[9-11] Platinum can increase activity by increasing the reducibility of NiO species in close proximity to Pt; H and CO form on Pt and spill over to reduce NiO.[12] Additionally, Pt has been shown to limit coking, so that more active surface area is available for reaction.[13] Islands of Pt on the Ni surface or Pt in a surface alloy decrease the ensemble size of Ni

regions and thus limit coking, which is more prevalent on larger Ni particles. Platinum also limits the amount of carbon whisker growth due to the low solubility of carbon in Pt and the low adsorption strength of carbon on Pt compared to Ni.[3, 14] Carbon whiskers grow on Ni when carbon diffuses across the surface and through sub-surface layers to find favorable step-edge facets from which to grow.[3] According to previous DFT calculations, the barriers for diffusion across the surface (137 kJ/mol) and subsurface diffusion (150 kJ/mol) are much smaller than the 225 kJ/mol barrier for carbon diffusion in bulk Ni. [15]

Typical Ni and NiPt bimetallic catalysts have been prepared by precipitation, incipient wetness impregnation, microemulsion, or other solution-based techniques.[9, 10, 13] In the current study, Ni and NiPt bimetallic catalysts for the DRM reaction were synthesized by atomic layer deposition (ALD) with the goal of increasing the activity and resistance to coking over traditionally-prepared catalysts. Aaltonen *et al.* first deposited Pt films by ALD using hundreds of cycles of $Me(Me_3Cp)Pt$ and O_2.[16] Since that time, much research has focused on creating Pt nanoparticles with less than 10 cycles of Pt ALD on metal oxide supports.[17-20] Ruthenium, Pd, RuPt, and PdPt bimetallic catalysts were also deposited on metal oxide supports using ALD in recent years.[21-23] With the exception of one study of Pt ALD that used H_2 as the second half-cycle reagent,[19] all other noble metal nanoparticle formation by ALD used O_2 or formalin.[18, 20-24] Previous work demonstrated recently[25] that Ni ALD could also be performed with H_2.

In the present study, catalysts with approximately 2.4 nm Ni particles were synthesized by ALD, and their performance in DRM was compared to catalysts prepared by IW impregnation. The ALD-prepared catalysts had higher DRM rate per g-metal because of a higher active surface area. They also exhibited enhanced coking resistance. Catalysts prepared by ALD did not form carbon whiskers after 72 h of reaction at 600°C, whereas IW-prepared Ni catalysts readily formed these carbon whiskers. Catalysts with even higher activity, stability, and coking resistance were prepared by adding Pt with

ALD to create bimetallic catalysts with high dispersions to maximize the bimetallic effect. We characterized the structure of bimetallic NiPt ALD catalysts using temperature-programmed studies, microscopy and specific chemisorption. Although the benefits of adding Pt to Ni DRM catalysts using methods other than ALD are known, reasons for the enhanced performance are not well understood, and thus DFT was used to elucidate why these structures provide enhanced DRM activity and coking resistance.

2. Experimental Methods

2.1 Catalyst synthesis. Nickel and Pt particles were formed on alumina supports by ALD. Two alumina supports were used: a nonporous alumina (Aldrich 544833 gamma alumina, ~40 m^2/g BET surface area, ~45-nm diameter spheres) and a porous gamma alumina (Albemarle MARTOXID AN/I, ~150 m^2/g BET surface area, ~75-μm particle diameters). The Ni ALD was performed in a stainless steel fluidized bed reactor (FBR) described elsewhere.[25, 26] The Pt ALD was performed in a quartz tube FBR (6-mm inner diameter) with a quartz glass frit of 40-μm pore size that supported the powder bed. The powder was fluidized in this reactor at approximately 0.25-Pa pressure with He carrier gas flow rates of 5 to 20 sccm. Platinum was deposited at 175°C, which is much lower than the typical 300°C used for Pt ALD with $Me_3(MeCp)Pt$ and O_2.[18, 19, 24] In this work, H_2 was used as the second reagent instead of O_2 for both Ni and Pt ALD. For bimetallic Ni + Pt ALD catalysts, the Ni particles were first deposited by incipient wetness (IW) impregnation or by ALD. Details of the IW and ALD Ni synthesis are explained in previous work.[25] The Ni catalysts were dried for 2 h under vacuum at 120°C before Pt was deposited by ALD in the quartz FBR. A bimetallic NiPt catalyst was also

synthesized by sequential IW impregnation (Ni followed by Pt) using the same methodology as the Ni IW synthesis, but using $H_2Pt_2Cl_6 \cdot 6H_2O$ as the metal precursor instead of $Ni(NO_3) \cdot 6H_2O$.

2.2 Catalyst Characterization. The catalysts were characterized by temperature-programmed studies in a quartz tube reactor (6.35-mm inner diameter) at ramp rates of 60°C/min and the effluent from the reactor was analyzed with an SRS RGA 200 mass spectrometer. For TPR, the catalysts were first oxidized for 2 h at 300°C and then cooled to room temperature in inert gas. The temperature subsequently was ramped in 50 sccm of 2.5% H_2 (balance Ar) while the H_2 uptake was measured with the mass spectrometer. For CO TPD, the catalysts were reduced for 2 h at 400°C, then cooled to room temperature, dosed with CO (50 sccm 20% CO in Ar) for 10 min, and then purged with Ar before ramping the temperature. In the case of post-reaction CO TPD experiments, the catalysts were reacted as normal, then cooled to room temperature before dosing CO. Diffuse reflectance infrared Fourier transform spectroscopy (DRIFTS) experiments were carried out using Thermo Scientific Nicolet 6700 FT-IR with a closed cell attachment (Harrick).

Transmission electron microscopy (TEM) was used to estimate catalyst particle sizes and determine the type of carbon deposited on the surface. Particle size estimates were obtained using Image J software to analyze images from an FEI Tecnai 12 - Spirit Biotwin TEM and a Phillips CM-100 TEM. (More details, including particle size distribution can be found in the supplemental information). Samples were electrostatically adhered to copper grids with a lacey carbon over-layer (Ted-Pella 01895 Lacey Carbon Film grids) to avoid effects of solvents from dropcasting. Samples prepared for imaging purposes were synthesized using the same methodology as previously mentioned, but a nonporous nanosphere alumina (Aldrich 544833 gamma alumina) was used so that the metal catalyst was on the surface of the spheres.

The weight loadings of each sample were determined by inductively coupled plasma mass spectroscopy (ICP-MS) of samples digested in a concentrated $HF/HNO_3/HCl$ solution for over 24 h.

The number of active sites was measured with a Quantachrome AS-1 Autosorb. The catalysts were reduced at 600°C in pure H_2 for 2 h before measuring the H_2 uptake to simulate the approximate surface area of these catalysts under reaction conditions. The active metal surface area and particle diameters were not estimated for bimetallic samples because the surface composition must be known in order to attribute chemisorbed H_2 to Ni or Pt; instead the H_2 uptake is reported.

The Ni ALD catalyst was prepared with one ALD cycle on both porous and nonporous spherical alumina as described previously.[25] The Ni weight loadings of the ALD and IW catalysts were similar at 4.7 and 6 wt%, respectively, but the particle size of the as-synthesized catalysts differed significantly at 2.4 nm for the ALD catalyst [25] and 17 nm for the Ni IW catalyst. High-temperature reduction of the ALD catalyst resulted in some sintering. After the catalyst was held for 2 h at 600°C in 50% H_2, the average particle size obtained from TEM was 3.6+/-0.4 nm. This is similar to the particle size of 4.0 +/-

0.1 nm obtained from chemisorption after the same pretreatment (Table 1).

Table 1. Catalyst composition and chemisorption results

Catalyst	Weight loading		H_2 chemisorption	Active metal surface area	Particle size
	Ni (%)	Pt (%)	$\mu mol/g_{catalyst}$ ($\mu mol/g_{metal}$)	($m^2/g_{catalyst}$)	(nm)
Ni IW	6	-	31 (520)	2.4	17
Ni ALD	4.7	-	96 (2000)	7.5	4
Pt ALD	-	1	33 (3300)	3.2	1
Ni IW + Pt ALD	6	1	69 (990)	-	-
Ni ALD + Pt ALD	4.7	1	105 (1800)	-	-
Ni IW + Pt IW	6	1	34 (490)	-	-

Ambient-pressure X-ray photoelectron spectroscopy (AP-XPS) was performed at beamline X1A1 at the National Synchrotron Light Source at Brookhaven National Laboratory. The bimetallic sample used in the AP-XPS studies was prepared by depositing Ni on a Pt(111) crystal (Princeton Scientific) from a 2.0 mm Ni rod (Goodfellow 99.0%) using an electron beam evaporator (Specs EBE-1). Using a quartz crystal microbalance, the thickness of the deposited Ni was estimated to be 2.5 Å. The sample was held >0.5 mm from the 500 μm entrance aperture of the differentially pumped hemispherical analyzer (Specs Phoibos 150 NAP), which was placed at 70° with respect to the incident x-rays and 20° from the surface normal. All scans were taken with a photon energy of 540 eV.

After normalizing the XPS data to the ring current, analysis of the XPS peaks was performed using OriginPro 9.1. A Shirley background was subtracted,[27] and the scans were adjusted to a reference Au foil such that the Au 4f peak was at 84.0 eV. Peaks were fit using a pseudo-Voigt function that was

approximately 50% Lorentzian and 50% Gaussian, with the fitting parameters (other than the area and center) constrained to be nearly constant for a particular element.

2.3 Reaction Studies. The catalysts were evaluated for DRM activity in a quartz tube, packed bed reactor (6.35-mm ID). The catalysts were reduced for 2 h at 400°C in 10% H_2 (balance Ar), with the exception of the IW catalyst, which was reduced at 500°C before reaction to ensure the particles were fully reduced after they were calcined at 550°C during synthesis. All catalysts were heated to 600°C and held at that temperature for approximately 10 min before the reactants were introduced to the reactor. Effluent gases were analyzed by a SRI 8610c GC with a Haysep-D packed column. Gas flow rates were 20 sccm CH_4, 20 sccm CO_2, and 60 sccm Ar. The amount of catalyst in the bed was varied (typically 50 to 200 mg) to achieve similar initial CH_4 conversions (35 to 40%). The amount of catalyst, total volumetric flow rate, and CH_4 and CO_2 concentrations were similar to those used in several Ni-based DRM studies.[6, 9, 10, 13, 28, 29] Rates reported represent the average rate throughout the bed, and comparison to literature values was done by using reported values of conversion, flow rates, weight loadings, and the catalyst weight to calculate the rate in terms of L $CH_4 \cdot h^{-1} \cdot g_{metal}^{-1}$. Most reactions were run for 12 h, but some were run for up to 72 h. At the end of the reaction time, the reactant flow was stopped and replaced by inert carrier gas before cooling the catalysts in order to avoid additional carbon deposition as the reactor cooled.

2.4 Density Functional Theory Calculations. The Vienna ab initio Simulation Package (VASP)[30, 31] was used to perform plane-wave DFT calculations. The plane-wave basis set was cut off at 396 eV, and reciprocal space was sampled with a 7x7x1 grid. The projector-augmented wave method[32, 33] was used for core electrons, and spin polarization was used in all calculations. A 3x3 surface cell and four metal layers were used, with the bottom two fixed and the top two allowed to relax. Further details are identical to those in a previous publication.[34] The lattice constant for the NiPt bulk alloy in a ratio

of 1:1 was found to be 0.381 nm. Although the materials used in this study are Ni-rich, using the bulk alloy lattice constant instead of Ni lattice constant (0.352 nm) did not significantly affect adsorption energies. For example, the methyl adsorption energy on a Ni/Pt/Ni(111) surface was -2.34 eV compared to -2.38 eV on at Ni/Pt/NiPt(111) surface.

A phase diagram was generated using atomistic thermodynamics, as described in detail in previous work.[35, 36] Briefly, the most stable surface structure at a given set of chemical potentials is the one that minimizes the surface energy:

$$\gamma(T,p) = \gamma_{clean} + \frac{E_{ads}}{A_{surf}} - \sum_i \frac{N_i \Delta\mu_i(T,p)}{A_{surf}} \qquad (1)$$

The number of each species in the surface unit cell, N_i, is defined by the surface structure, while the chemical potentials $\mu_i(T,p)$ are variables that depend on the temperature and pressure:

$$\mu_i(T,p) = \mu_0(T,p^0) + kT\ln(\frac{p^i}{p^0}) \qquad (2)$$

Several simplifications were made to make the phase diagram generation tractable. First, only two metal structures were considered: (i) a pure Pt top layer, a pure Ni subsurface layer, and NiPt bulk layers (Pt/Ni/NiPt); or (ii) a pure Pt top layer, a pure Ni subsurface layer, and NiPt bulk layers (Ni/Pt/NiPt). Previous work has shown that one of these two metal structures is the most stable under most O_2 chemical potentials.[36] Since these two structures have the same number of Pt and Ni atoms, terms that depend on N_{Pt} and N_{Ni} were not included in Equation 1.

Since the transition between the surface terminations occurs at a low coverage[36] (see Figure 3 below), only structures with 4/9 ML or less of combinations of C, CO, and O were considered. Their surface chemical potentials were calculated as:

$$\mu(O^*) = \mu(CO_2) - \mu(CO)$$

$$\mu(CO^*) = \mu(CO)$$

$$\mu(C^*) = \mu(CO) - \mu(O^*)$$

$$= 2\mu(CO) - \mu(CO_2)$$

Chemical potentials denoted with an asterisk indicate surface species; all other species are in the gas phase. Gas-phase chemical potentials are referenced to the isolated molecules. To account for coverage effects, adsorption energies calculated at 1/3 ML were used, but otherwise adsorbate-adsorbate interactions were ignored. Since only surface structures with a single type of adsorbate were found to be stable in the conditions tested, this is likely to be a good approximation.

3. Results and Discussion

3.1 Nickel Catalysts.

Nickel catalysts synthesized by incipient wetness (IW) and ALD techniques were evaluated for the DRM reaction. All IW-synthesized catalysts reached steady state within the first hour, but the Ni ALD catalysts took up to 25 h to reach steady state, as shown in Figure 1. The CH_4 reforming rate at 600°C (normalized per g_{metal}) at steady state for the Ni ALD catalyst was at most 1.7 times that for the IW Ni catalyst (using a t-test with α=0.05). Correspondingly, the metal surface area of the Ni ALD catalyst (calculated using post-reaction particle size measured by TEM)[25] was approximately 1.5 +/- 0.1 (at a 95% confidence) times higher than the IW catalyst surface area determined from chemisorption. Thus, the higher rate appears to be due primarily to the higher metal surface area (calculated from post-reaction particle size). However, comparing DRM rates normalized by surface area can over-represent the number of surface sites when carbon blocks an indeterminable number of sites. For this reason, we compare DRM rates normalized per gram-metal to avoid assumptions of rates normalized by surface area.

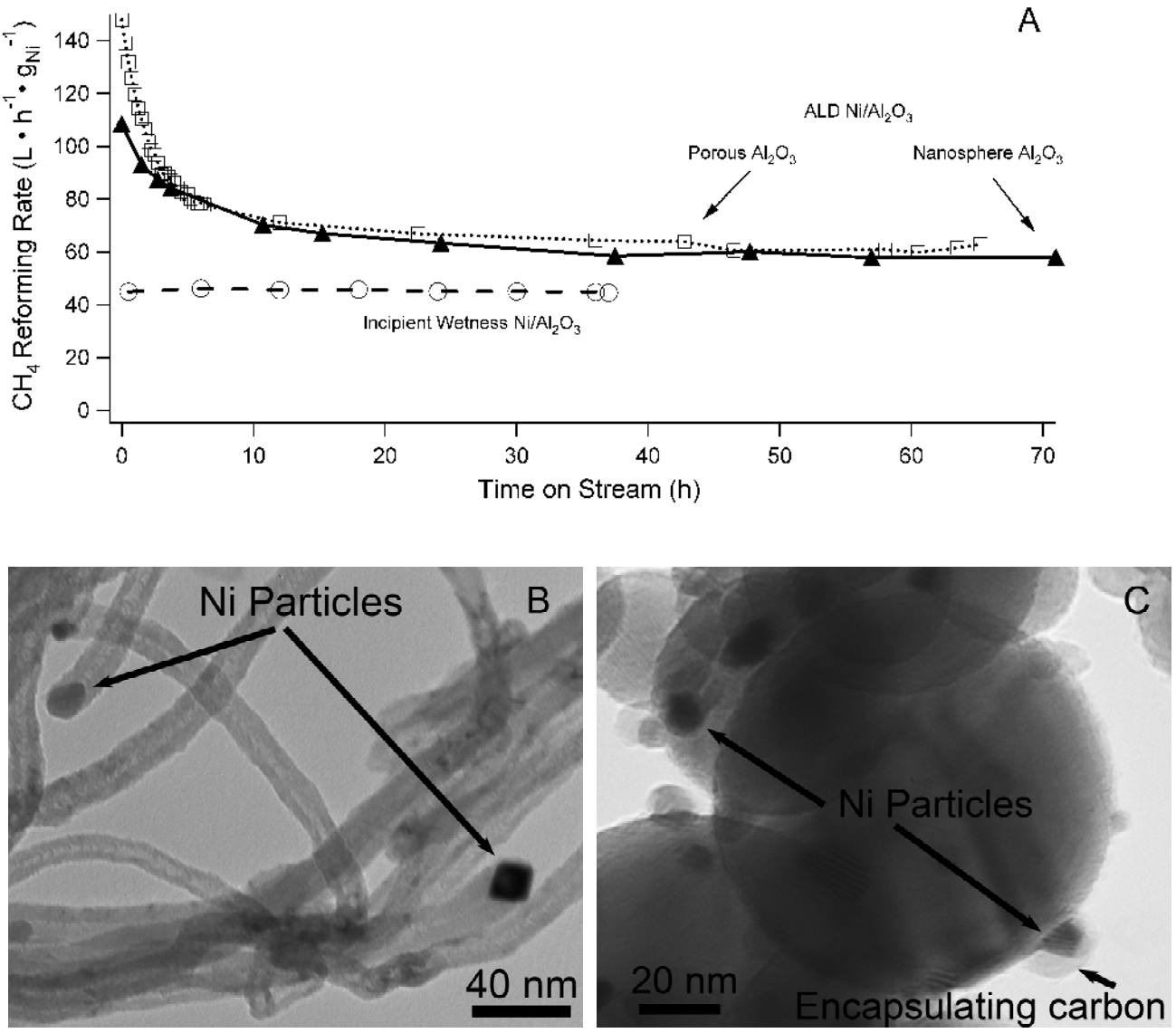

Figure 1. A) DRM reforming rates as a function of time for Ni IW and Ni ALD catalysts at 600°C. Both porous and nanosphere Al_2O_3 supports were used for the Ni ALD catalysts. B) TEM image showing carbon whiskers on the Ni IW catalyst supported on porous Al_2O_3 after 36 h on-stream. C) TEM image of Ni ALD catalysts on nonporous Al_2O_3 spheres after 72 h of DRM at 600°C.

The Ni ALD catalyst not only had a higher average DRM rate (60 L $CH_4 \cdot h^{-1} \cdot g_{Ni}^{-1}$) than the IW catalyst (31 L $CH_4 \cdot h^{-1} \cdot g_{Ni}^{-1}$), it also had a higher rate than Ni catalysts in the literature; those rates were 10 to 25 L $CH_4 \cdot h^{-1} \cdot g_{Ni}^{-1}$ at 600°C under similar flow rates and pressures.[10, 13] Nickel/Al_2O_3 IW

catalysts investigated in this study had a higher rate than other Ni/Al_2O_3 catalysts reported in literature due to their lower weight loading and higher dispersion. The Ni ALD catalysts also had higher rates than a Ni/Mg(Al)O catalyst (5-6 nm Ni particles from a hydrotalcite-derived synthesis),[37] which had reforming rates of 43 L $CH_4 \cdot h^{-1} \cdot g_{Ni}^{-1}$ at similar conditions.[29] However, the Ni ALD catalysts had lower rates than similar-sized (2 nm initially) Ni nanoparticles of a $Ni(Si_xO_z)/CeO_2$ catalyst, which had a DRM rate of 270 L $CO \cdot h^{-1} \cdot g_{Ni}^{-1}$ (which corresponds to ~100 to 135 L $CH_4 \cdot h^{-1} \cdot g_{Ni}^{-1}$ depending on the H_2 to CO ratio) after 43-h reaction time.[38] Note that the steady-state rate for the Ni ALD catalysts in Fig. 1 was only reached after about 25 h, during which time the catalyst lost 59 to 67% of its activity, as shown in Figure 1a. The Ni ALD catalyst was then stable for up to 72 h at 600°C. Another Ni ALD sample was run for a longer period of time, losing ~ 60% of its activity within the first 25 h, and then only losing 4% activity over the next 175 h. The Ni ALD activity loss during DRM at 600°C.was smaller than that observed by Baudouin et al. (80 to 90 %) when they used Ni/SiO_2 catalysts with initial particle diameters from 1 to 7 nm for DRM at 500°C.[28] The Ni ALD catalysts in the current study deactivated similarly to a 2.1-nm $Ni(Si_xO_z)/CeO_2$ catalysts that deactivated by 55% after 43 h.[38] The ALD catalyst particle diameters measured by TEM were 3.5 +/- 0.7 nm after 2-h reduction in 10% H_2 at 400°C, and during reaction they sintered to 9.4 +/- 2.4 nm (size distribution shown in Supplementary Information Figure S1), which corresponds to a 39 to 77 % surface area loss. The activity loss over time appeared to be characteristic of particle sintering, so we modeled the reaction rate loss as being proportional to active surface area loss, as described by Bartholomew.[39] The decrease in surface area of transition metals due to sintering is known to follow power-law kinetics:

$$\frac{d}{dt}(A_{Ni}) = k(A_{Ni})^n \qquad (3)$$

where A_{Ni} is the surface area of the Ni catalyst, and k is the rate constant.[2, 39, 40] If we assume deactivation was solely due to a change in surface area, the reaction rate data in Figure 1a can be fit to

the above power law, yielding a value of n = 7.5. This value of n is within the particle coalescence regime (n ≈ 8 or greater), as opposed to the atom migration sintering regime (2 < n < 5).[2, 4, 39, 40]

Although the Ni ALD particles sintered, they were still smaller than the IW Ni particles (approximately 17 nm both before and after reaction), and their small size may have limited the amount or type of coke deposition. No carbon nanotubes (whiskers) were detected by TEM on the Ni ALD catalyst after reaction, whereas the Ni IW catalyst had carbon nanotubes deposited throughout the sample after 36 h of reaction, as shown in Figure 1b. Although the reaction rate was stable for the IW catalyst, at longer times the carbon whiskers would be expected to eventually plug the reactor or destroy the catalyst particles. These carbon deposition results are similar to those found in the TGA study by Beengard *et al*. that showed when n-butane flowed over Ni catalysts while the temperature was ramped, coking began at a temperature 100°C higher and at a slower rate on 7-nm Ni particles than on 107-nm Ni particles.[5]

The Ni ALD particles shown in Figure 1 did not grow large enough to nucleate carbon whiskers after 72 h of reaction, but instead appeared to have thin layers of encapsulating carbon as shown in Figure 1c. This suggests that operating under reaction conditions can help limit sintering to the critical carbon formation size. Particle migration and coalescence has been described as a surface-mediated transport of Ni atoms and Ni-OOH complexes from one side of the particle to the other.[4, 40] To test the importance of particle size in the formation of carbon whiskers, we pre-sintered a Ni ALD catalyst for 24 h at 600°C in 20% H_2 and then ran the DRM reaction. This pre-sintered sample formed carbon whiskers instead of encapsulating carbon, as shown in Supplementary Information Figure S2. The carbon whisker diameters (17.5 +/- 5.3 nm) were used as an approximation of the effective particle size,[3, 41, 42] indicating that these pre-sintered particles sintered to larger sizes under reaction conditions than the regular Ni ALD sample.

3.2.1 Nickel-Platinum ALD Catalyst Materials Characterization. The nickel catalysts described above were used to create bimetallic catalysts by adding Pt by ALD or IW techniques. The Pt ALD deposited extremely small particles (approximately 1 nm) so that one ALD cycle added significant active surface area to the Ni IW catalyst, whereas Pt addition by IW added little surface area. The Pt ALD did not significantly increase the surface area of the Ni ALD catalyst (as indicated by a slight decrease in the H_2 chemisorption uptake after Pt ALD), which was consistent with forming bimetallic particles rather than nucleating new particles. Weight loadings and chemisorption uptakes for each catalyst are listed in Table 1.

Temperature-programmed reduction (TPR) was performed to gauge bimetallic interaction of the catalysts (Figure 2). Monometallic catalysts were also investigated with TPR, and the Ni ALD catalyst exhibited a lower reduction temperature than larger Ni IW particles. The main H_2 uptake peak of the PtNi catalysts was between the peaks for the single-metal catalysts; this indicated the Pt was in close proximity to the Ni. This intermediate-temperature peak results by reducing a NiPt alloy or by Pt providing dissociated H for reducing nearby NiO species.[43] However, the peaks for the single-metal catalysts are also present in Figure 2 for the IW Ni catalyst modified with Pt ALD, suggesting that the catalyst was composed of isolated Pt and Ni particles or regions and NiPt alloy particles. Previous work by Jentys *et al.* used X-ray adsorption techniques to verify that a TPR of a Ni-rich NiPt catalyst will exhibit a much higher temperature reduction peak when Ni is not in a bimetallic phase with Pt.[44] The NiPt catalyst synthesized entirely by ALD did not show much monometallic character however, indicating a higher degree of bimetallic interaction.

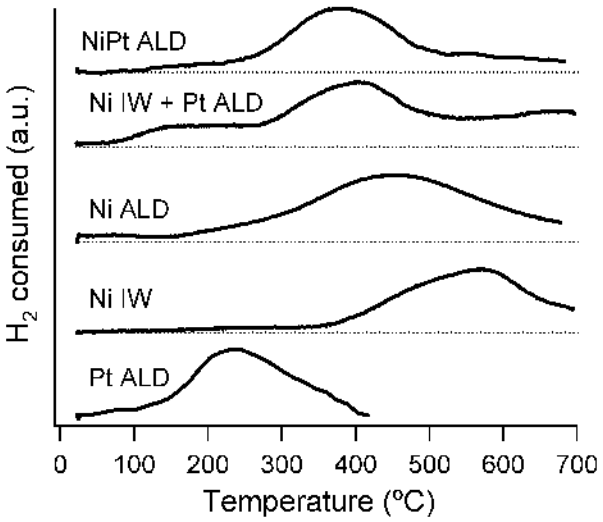

Figure 2. Hydrogen uptake of Ni, Pt, and NiPt catalysts obtained by temperature-programed reduction.

The structure of the bimetallic catalyst can change under reaction conditions, depending on which gases adsorb on the metal surface. Nickel-platinum bimetallic layers have been shown to change which metal terminates the surface depending on which gas adsorbed.[12, 45] Probing the catalyst surface structure with *in-situ* techniques is difficult under the harsh conditions associated with DRM. Instead, we used DFT to analyze how the surface energy of different terminations varied as a function of coverage for multiple adsorbates associated with the DRM reaction. Previous work[36] has shown that for oxygen adsorption, the surface consists of either a pure Pt or a pure Ni top layer, depending on the oxygen chemical potential. Therefore, only the Pt/Ni/NiPt and Ni/Pt/NiPt structures were examined. As shown in Figure 3, the Pt-terminated surface is more favorable at low adsorbate coverages, but the difference becomes smaller as the coverage of any adsorbate increases. The surface Pt termination is predicted to change to a Ni termination at low coverages of O or C, moderate coverages of CO, and high coverages of H.

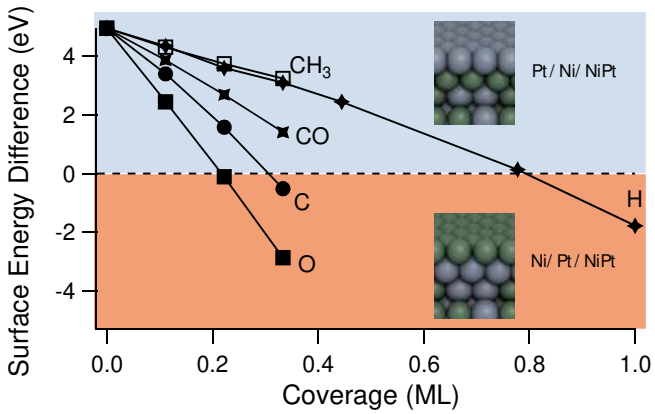

Figure 3. Adsorbate dependent surface termination of Ni-Pt bimetallic surfaces, where a positive value indicates that Pt/Ni/NiPt is more favorable and a negative value indicates that Ni/Pt/NiPt is more favorable. Insets show metallic structures that were used for the DFT calculations. The values on the y-axis represent eV/unit cell area.

A phase diagram for the surface structure at different CO and CO_2 chemical potentials was also calculated, as shown in Figure 4. Under the experimental reaction conditions, the surface is predicted to be Ni-terminated and covered with atomic C. At low chemical potentials of both CO and CO_2, the surface is predicted to be Pt-terminated and bare, while at low CO_2 chemical potential the surface can be Pt-terminated with adsorbed CO, Pt-terminated and bare, or Ni-terminated with adsorbed O, depending on the CO chemical potential. Previous work on aqueous phase reforming of ethylene glycol on Ni-Pt catalysts also indicated that mostly Ni is on the surface under reaction conditions[45].

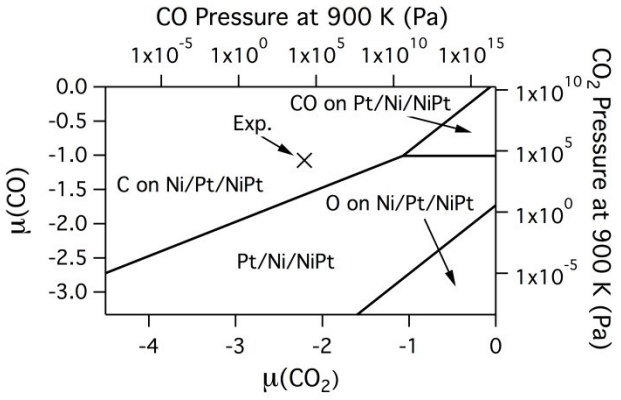

Figure 4. Phase diagram for NiPt bimetallic surfaces as a function of the CO and CO_2 chemical potentials. The "X" denotes representative chemical potentials of the adsorbates during the experiments in this work assuming atmospheric total pressure.

As an additional check on the DFT results, the surface structure was experimentally probed on a NiPt ALD catalyst. The catalyst surface during (and probably after) the DRM reaction conditions likely has significant amounts of surface C,[46, 47] which favors a Ni-terminated bimetallic surface as shown in Figure 4. Carbon monoxide TPD was performed on a fresh (reduced 2 h in 20% H_2 at 400°C) NiPt ALD catalyst and on a catalyst exposed to reaction conditions for 12 h at 600°C. The CO TPD, shown in Figure 5, has two peaks for the fresh sample, but only one peak after reaction. The peak around 100°C is representative of the α_1 single-site CO desorption mode on Pt and the higher temperature peak corresponds to a β_2 CO associative desorption mode from kink and step sites of Ni.[43, 48] The Pt-related α_1 peak disappeared after reaction, indicating that those Pt sites were no longer available on the surface to bind CO. This Pt-related α_1 peak disappearance was not likely due to C covering the Pt sites. Our calculations show that Pt-terminated surfaces exhibit larger C diffusion barriers (0.61-0.69 eV) than Ni-terminated surfaces (0.10-0.50 eV), and that Pt-terminated surfaces have a less favorable C

adsorption energies (-5.9 eV) than that of a Ni-terminated surface (-7.5 eV). Carbon on the bimetallic samples would thus be expected to preferentially form on the Ni regions and not diffuse to Pt metal sites or Pt-terminated bimetallic sites. Platinum weight loading of the post-reaction sample was confirmed by ICP-MS, indicating that the Pt was still in the sample at the original weight loading, just not on the surface. To ensure that the differences in CO desorption were due to reactant exposure and not high temperature, a NiPt ALD catalyst was reduced for 2 h at 400°C in 20% H_2, then held at 600°C in Ar for 12 h before running the CO TPD. This TPD showed both the low-temperature Pt peak and the high-temperature Ni peak, indicating that the disappearance of the Pt peak was not due to thermal treatment. Surface area loss and perhaps surface carbon were responsible for the decreased β_2 desorption peak after reaction. These TPD results agree with our findings from DFT that the surface was Ni-terminated during reaction, but the effect of sintering on the disappearance of the low-temperature peak could not be ruled out.

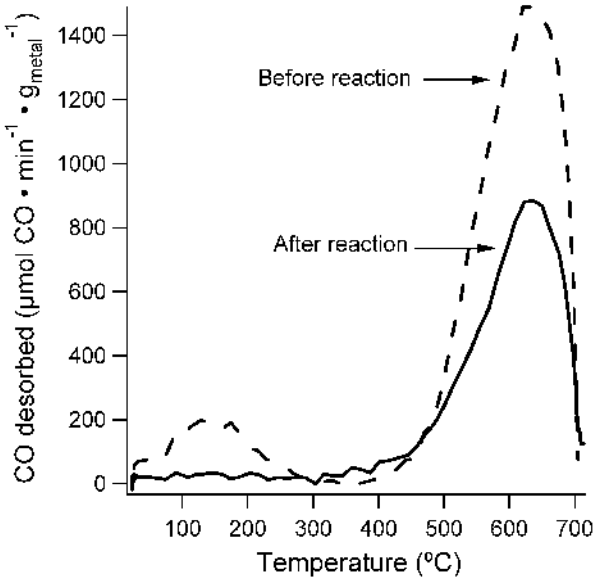

Figure 5. Carbon monoxide temperature-programmed desorption of Ni-Pt ALD catalysts before and after reaction.

To better characterize the role of reaction conditions in changing surface composition, we also conducted AP-XPS experiments on a Pt(111) single crystal with an overlayer of Ni. In some ways, such a system represents the inverse of the Pt/Ni catalysts prepared by deposition of Pt on a Ni-containing catalyst. However, this system has been extensively studied in previous work; this work has shown that the surface composition of the Ni/Pt(111) system varies strongly depending on exposure to oxidizing or reducing conditions. [49] After depositing approximately 2.5 Å of Ni on the Pt(111) crystal, mild annealing at 200 °C for 5 minutes was performed to generate a smooth Ni overlayer.[49] To ensure a fully Ni-rich surface as a baseline spectrum (Figure 6(a)), O_2 was dosed at 2.7 x 10^{-5} Pa and the sample was held at 200 °C for 30 min, and then held at 227 °C in 4.3 x 10^{-5} Pa for 30 min. Over the course of this treatment, the XPS scans showed little change from the annealed scan. A short annealing step at 227 °C in vacuum decreased the Ni/Pt ratio to 1.05. Next, CO_2 and CH_4 were dosed in a 1:1 ratio (total pressure of 130 Pa) and the temperature was raised in steps to 350 °C over the course of 90 min. This treatment increased the Ni/Pt ratio to 1.47 at 250 °C (Figure 6(b)), indicating a surface enrichment in Ni caused by the reaction conditions. As temperature was increased, the Ni/Pt ratio was gradually decreased to 1.04 at 350 °C. This decrease in surface enrichment is consistent with an entropic effect driving Ni into the subsurface or bulk. It was noted that during exposure to CO_2 and CH_4, the C 1s peak shape changed significantly, indicating that reaction had taken place and deposited some type of C-containing species on the surface.

As a next step, 2.7 x 10^{-5} Pa of H_2 was added to the chamber, the sample was slowly heated to 400 °C over the course of 60 minutes, and then the pressure was increased to 4.3 x 10^{-5} Pa. This dramatically decreased the Ni/Pt ratio to 0.53, indicating a decrease in Ni coverage, consistent with results from prior work. *[50]* Finally, the CO_2 and CH_4 were reintroduced at the same pressures as before, and the temperature was slowly increased from 250 °C to 400 °C over the course of 45 minutes.

The Ni/Pt ratio rose to 0.62 at 300 °C, indicating that some subsurface Ni was coming back to the surface. At 400 °C, the ratio decreased to 0.58 and appeared to stabilize. Care must be taken when comparing the results of these studies on a Ni/Pt(111) surface to Ni-rich bimetallic catalysts, where both the catalyst surface and reaction conditions are different. Most importantly, in the single crystal studies, at high temperatures there is a strong driving force for Ni to diffuse into the Pt crystal bulk because of its very low atom fraction, limiting the ability to probe true reaction conditions on such a substrate. In contrast, the supported Ni-rich catalysts have a large reservoir of Ni to populate the surface. Nevertheless, the results are consistent with a tendency for the CO_2/CH_4 gas environment to increase the Ni content of the surface, consistent with our DFT and experimental results. The growth of the C 1s XPS peak intensity after exposure to CO_2 and CH_4, (as shown in Supplementary Information Figure S3) is consistent with the surface segregation occurring due to C deposition. The binding energy of ~285 eV was representative of graphitic-like carbon, similar to the major carbon feature observed by Pawalec *et al.*[11]

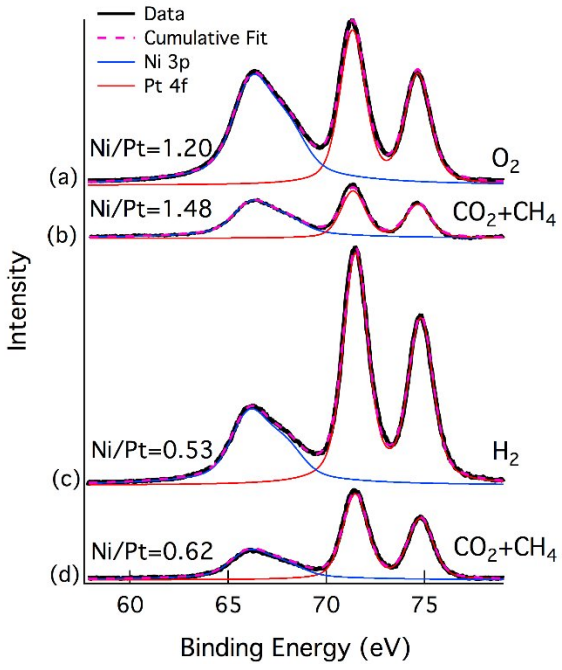

Figure 6. *In-situ* XPS spectra for (a) a Ni-Pt crystalline surface (a) exposed to O_2 (4.3×10^{-5} Pa pressure) for 30 min at 227 °C; (b)) subsequently annealed to 250 °C in an equimolar mixture of CO_2 and CH_4 (130 Torr total pressure); (c) subsequently annealed to 400 °C in H_2 (4.3×10^{-5} Pa pressure); and (d) subsequently annealed to 300 °C in an equimolar mixture of CO_2 and CH_4 (130 Torr total pressure). See the main text for the full details of the experimental sequence.

We also characterized the evolution of the catalyst surface following high-temperature exposure to reactive gasses using infrared spectroscopy. Because our DRIFT cell was not equipped to operate under the demanding conditions of the reaction, we instead conducted these experiments under milder conditions designed to test the tendency of Ni to segregate to the surface. Both PtNi and Ni catalysts prepared by ALD were exposed to 2 Torr CO near room temperature, during heating to 540 K, and during subsequent cooling to low temperature. Our hypothesis was the high-temperature exposure to a strongly-adsorbing gas would cause surface enrichment in Ni on the PtNi catalyst, and that this termination would be preserved during subsequent cooling to room temperature. We indeed observed a change in the vibrational signature for adsorbed CO as a result of the heat process on PtNi, but not on Ni catalyst (see Figure S4 of the Supplementary Information). Although interpretation of these complex spectra is not straightforward, the results are consistent with a compositional change in the surface that occurs at higher temperature.

3.2.2 NiPt DRM reactivity. Modifying Ni catalysts with one cycle of Pt ALD increased the average DRM rate by a factor of at most 1.7 for the Ni ALD catalyst and 2.4 for the Ni IW catalyst (using a t-test with α=0.05), as shown in Figure 7. A catalyst containing Pt deposited by one ALD cycle had a higher

initial activity than that of the Ni ALD catalyst, but as shown in Supplementary Information Figure S5, it deactivated within 1 h to the steady state value reported in Figure 7. de Miguel *et al*.[13] observed previously that Pt-only catalysts deactivated by 75 to 80% at 700°C within 6 h during the DRM reaction. The NiPt ALD catalyst had a stable reforming rate after 10 h, whereas the monometallic Ni ALD catalyst was only stable after 25 h.

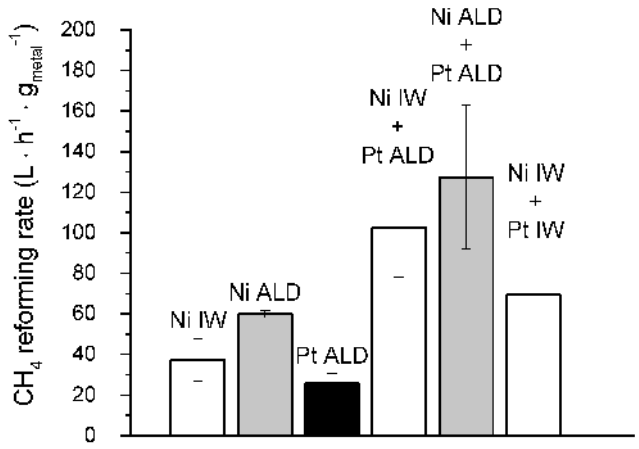

Figure 7. Steady-state rates of dry reforming of methane at 600°C normalized per gram of metal. The three bimetallic catalysts had Pt added to the two Ni catalysts shown on the left. Error bars represent standard deviation.

Adding Pt to the Ni catalysts by ALD increased the catalytic activity by more than the sum of each monometallic catalyst's activity, with each ALD bimetallic catalyst's rate being statistically higher than the summed monometallic catalyst rates (at α=0.075 for the Ni ALD + Pt ALD catalyst, and α=0.05 for the Ni IW + Pt ALD catalyst). A comparison of how adding Pt to a Ni catalyst affects the DRM rate is shown in Table 2 for our NiPt ALD catalyst and other NiPt catalysts from literature. In most cases, the effect of adding Pt to a monometallic Ni catalyst is relatively small compared to the larger effect observed for the ALD catalyst. However, the other bimetallic catalysts have lower ratios of Pt:Ni than the ALD catalyst. Another major factor affecting the rates shown in Table 2 is the size of the particles, but correlating reaction rates solely to the particle sizes is difficult since the weight loadings and the

support material also varies significantly between the catalysts. The improved performance of the NiPt ALD catalyst is likely due to a combined effect of the smaller particle size (which improves active surface area and the degree of bimetallic interaction), and a more ideal ratio of Ni:Pt.

Table 2. Comparison of DRM rates for Ni and NiPt catalysts.

Catalyst	Weight Loading (%)		Particle diameter (nm)		Temperature (°C)	CH_4 Conv. %	CH_4 Reforming Rate (CH_4 L · h^{-1} ·g_{metal}^{-1})	Ref.
	Ni	Pt	Initial	After reaction				
Ni ALD	4.7	0	3.5	9.4	600	12	60	This work
NiPt ALD	4.7	1	-	-	600	30	122	This work
Ni/ZSM-5	5	0	10	-	600	21	100	[11]
Pt_6Ni/ZSM-5	5	0.5	8.7	-	600	29	114	[11]
Ni(10%)/Al_2O_3	10	0	~22		750	70	25	[13]
Pt(0.5%)Ni(10%)/Al_2O_3	10	0.5			750	79	27	[13]
4Ni/Al_2O_3 IM	10	0	23	25	600	16	16	[10]
0.04Pt4Ni/Al_2O_3 IM	10	0.4	7	14	600	13	13	[10]

Nickel-platinum catalysts prepared in this work by sequential incipient wetness impregnation had a dry reforming rate of 61 L CH_4 ·h^{-1} ·g_{metal}^{-1}. This rate was lower than the ALD bimetallic catalysts (102 to 122 L CH_4 ·h^{-1} ·g_{metal}^{-1}), and was not statistically different (at α=0.75) from the Ni IW catalyst. During DRM, the H_2/CO product ratios (~0.5-0.6) were similar for all catalysts investigated except for the Ni ALD + Pt ALD catalyst, which had a slightly higher ratio (0.67) as shown in Supplementary Information Figure S6. These H_2:CO ratios are similar to other Ni, Pt, and NiPt catalysts reported in literature for DRM at 600°C.[10, 51]

DFT was used to understand why the bimetallic catalysts had superior DRM rates. Specifically, we investigated how bimetallic NiPt surfaces interacted with the different adsorbates found in the DRM reaction. Recent work by Jones *et al.* used first principles calculations and experimental investigations

to elucidate which pure metals would be most favorable for CH_4 steam reforming.[14] They found that Ru was the best reforming metal and that the high reforming TOFs were correlated with the C and O adsorption energies calculated for that surface. By applying the same principles, we used the O and C adsorption strengths on Ru as a benchmark to gauge which bimetallic catalyst surfaces would be more effective for dry reforming; i.e., a catalyst with C and O adsorption energies closer to those of Ru was deemed likely to be a superior catalyst. In addition to comparing the C and O adsorption energies, the dissociative CH_4 adsorption and CO formation energies were also investigated since these are the kinetically limiting steps.[14] Four surfaces, shown in Supplementary Information Figure S7, were used to model the PtNi bimetallic surfaces. As can be seen in Figure 8, the Ni-terminated alloy has similar adsorption properties to Ru, and the similarity is maintained (though lessened) if 1/3 of the atoms in the top layer of this surface are replaced with Pt. This is in contrast to Ni, Pt, and the Pt-terminated alloy (even with 1/3 ML of Ni in the surface), which bind O and C too weakly. As noted above, experimental investigation and theoretical prediction indicated that the Ni-terminated surface is present under reaction conditions.

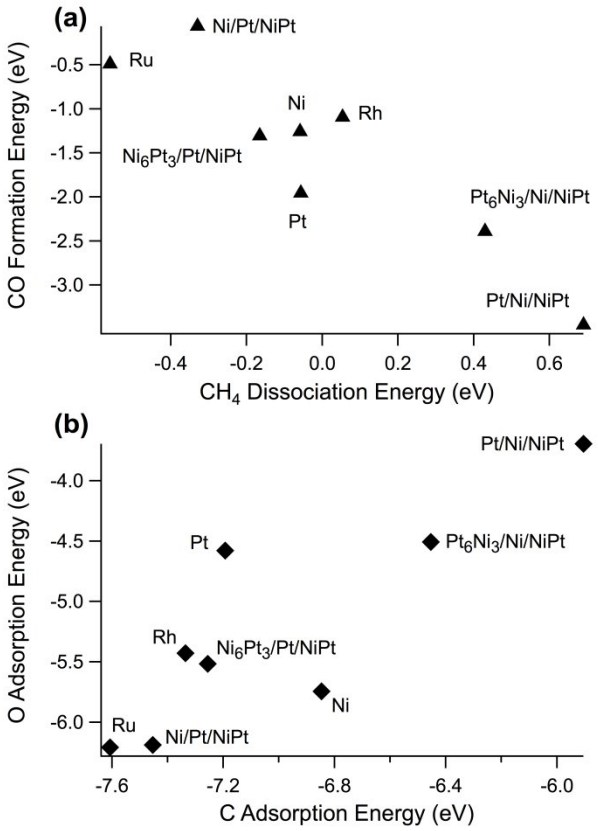

Figure 8. A) Carbon and oxygen adsorption energies of different metal surfaces. B) CO formation and CH_4 dissociation energies of different metal surfaces.

3.2.3 Carbon deposition on NiPt. The post-reaction TEM images of the NiPt ALD catalyst show the particles ranged from approximately 3 to 20 nm (with average particle size of 9.4 +/- 4.5 nm), as shown in Figure 9. The larger particles would be expected to form carbon whiskers if they were not bimetallic, though the smaller particles could be monometallic and still not form carbon whiskers. Analysis by TEM of post-reaction bimetallic ALD samples indicated only sparse carbon whiskers on the samples, as shown in Figure 9, but the IW-prepared NiPt catalyst still had a large number of carbon whiskers. The carbon whisker growth on the IW Ni + Pt IW catalyst was similar to that of the Ni IW catalyst, indicating that incipient wetness did not distribute Pt effectively on Ni particles, but ALD did. Platinum has been shown to decrease coking during dry reforming of methane on Ni-Pt bimetallic catalysts,[9, 11,

13] so the presence of carbon whiskers on the IW bimetallic catalyst is most likely due to large Ni-only catalyst particles or regions.

Temperature-programmed oxidation was used to characterize the amount of carbon deposited on the catalysts by measuring the amount of CO_2 produced. As shown in Supplementary Information Figure S8, the Ni IW + Pt IW catalyst had more than 2 orders of magnitude more carbon deposited than the Ni ALD + Pt ALD sample. This large discrepancy in carbon deposited was another indicator that Pt deposited by IW was not effectively dispersed and therefore did not limit coking the way Pt ALD did.

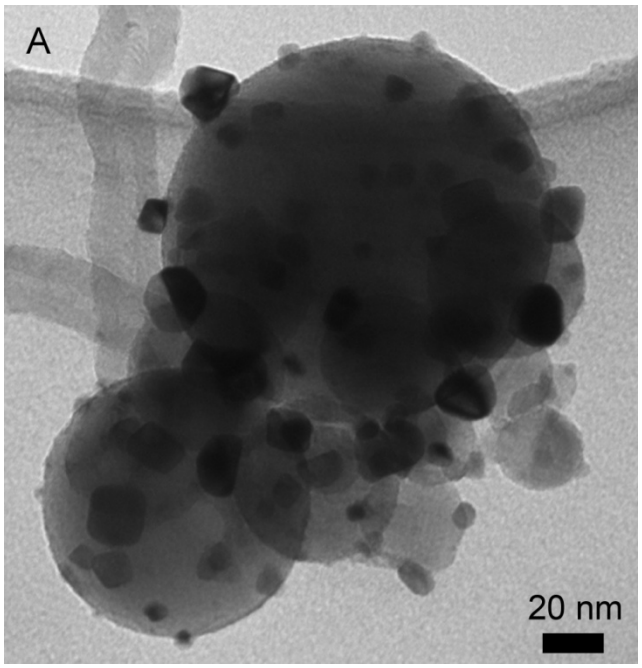

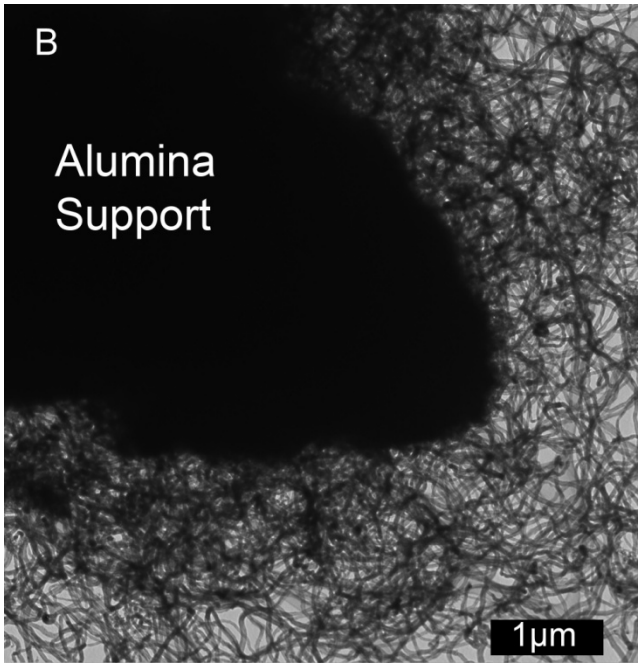

Figure 9. (A) Bimetallic NiPt ALD catalyst particles after 32 h of reaction at 600°C indicate varying particle sizes with minimal carbon whisker deposition. Metal particles (dark <20 nm) were supported on spherical alumina supports. (B) NiPt catalyst prepared by IW after 42 h of reaction show growth of carbon whiskers.

Density functional theory was used to explore possible explanations for the amount of carbon deposition on different catalysts. Importantly, whisker formation requires a much larger ensemble of contiguous sites than methane activation, so that whereas small quantities of surface Pt atoms would not be expected to strongly affect DRM activity, they may affect whisker growth. Our DFT calculations suggest that suppression of coking may be due to the presence of some Pt "defects" on the active surface. The tendency to coke likely depends on a number of factors, including the rate of C diffusion and the energetics of graphitic carbon formation.[15] In particular, the activation barriers for C diffusion have previously been used to explain the increased coke resistance of NiSn alloys.[52] Our climbing-image, nudged elastic band calculations of the barrier for diffusion from an fcc hollow to a neighboring hcp hollow on Pt gave an identical result as simply performing an adsorption calculation in the bridge

site. Therefore, we used the difference in adsorption energy between the bridge site and most stable site as a measure of the ease of carbon diffusion. The results (see Table 3) may explain why there is substantial coking on Ni but not on Pt, Ru and Rh: Ni has a much lower barrier to C diffusion. The Ni-terminated alloy also has a low barrier, but the coverage of 1/3 ML of Pt atoms in the surface layer significantly increases this barrier. At the high temperatures used in methane reforming, some Pt atoms may be on the surface, and these atoms may inhibit large-scale diffusion of C atoms.

Table 3. Barriers to Atomic Carbon Diffusion.

Surface	Diffusion Barrier (eV)
Ni	0.36
Pt	0.85
Ni/Pt/NiPt	0.10
Pt/Ni/NiPt	0.61
Ni_6Pt_3/Pt/NiPt	0.50
Pt_6Ni_3/Ni/NiPt	0.69
Ru	0.77
Rh	0.67

Since carbon preferentially nucleates at Ni step edges, we investigated the effect of replacing one Ni (211) step edge atom with a Pt atom. The calculated C adsorption energy (-7.45 eV) was weaker than the Ni (211) step edge C adsorption energy (-7.85 eV), indicating that Pt atoms near step edges may destabilize C nucleation. The same trend holds on the Ni-terminated alloy, Ni/Pt/PtNi(211); Pt at the step site destabilizes C by 0.07 eV, making it nearly equal to the adsorption energy on the Ni/Pt/PtNi(111) terrace (-7.45 eV). Therefore, surface Pt atoms inhibit C diffusion across the terraces and destabilize C adsorption at the step site, both of which may inhibit coking.

4 Conclusions

Nickel catalysts prepared by atomic layer deposition (ALD) had higher rates per g-metal for dry reforming of methane (DRM) than larger Ni particles synthesized by incipient wetness. These Ni ALD catalysts also inhibited the growth of carbon whiskers during reaction because the Ni particles were ~ 8 nm smaller than the IW catalyst particles, even after sintering. Adding Pt to the Ni catalysts by ALD increased the catalytic activity by a factor of approximately two, and the activity of these catalysts (on a per gram metal basis) was higher than NiPt DRM catalysts reported in the literature because of the small size of these particles. Also, less carbon deposited on the NiPt ALD catalysts than on all other catalysts investigated. Temperature-programmed reduction suggested these NiPt catalysts contain both bimetallic and individual metal nanoparticles. Results from DFT calculations indicated that the NiPt catalyst surface was Ni-terminated under reaction conditions because adsorbates bring Ni to the surface, and the tendency for DRM conditions to increase surface Ni content was confirmed by AP-XPS. These Ni-terminated catalysts were predicted to perform better than Pt-terminated bimetallic catalysts or the individual metals. Bimetallic catalysts may have coked less because of the higher C diffusion barrier on terraces and weaker C adsorption energy at step edges where Pt is present. These ALD catalysts performed better than most DRM catalysts reported in the literature, likely because of their nanoscale features and maximized bimetallic interaction.

Author Information

Corresponding Author

*E-mail: Will.Medlin@Colorado.edu

Acknowledgments

The work was supported through the National Science Foundation Graduate Research Fellowship Program and NSF Grants CBET 1067800 and CBET 0854251. The authors thank Fred Luizer in the University of Colorado's Laboratory of Environmental and Geological Studies (LEGS) for conducting ICP-MS analysis. The authors also thank Tom Giddings and the MCDB Bio3d Electron Microscopy

center for the use of TEM microscopes and sample preparation equipment. Special thanks to Sarah Gould for designing graphical art. We acknowledge supercomputing time at the Center for Nanoscale Materials at Argonne National Laboratory, supported by the U.S. Department of Energy, Office of Basic Energy Sciences, under Contract DE-AC02-06CH11357. A portion of the research was performed using EMSL, a national scientific user facility sponsored by the Department of Energy's Office of Biological and Environmental Research and located at Pacific Northwest National Laboratory.

References

[1] D.A. Wood, C. Nwaoha, B.F. Towler, Journal of Natural Gas Science and Engineering 9 (2012) 196-208.

[2] J.R. Rostrup-Nielsen, J. Sehested, J.K. Nørskov, Hydrogen and synthesis gas by steam- and C02 reforming, in: Advances in Catalysis, Academic Press, 2002, pp. 65-139.

[3] S. Helveg, J. Sehested, J.R. Rostrup-Nielsen, Catalysis Today 178 (2011) 42-46.

[4] J. Sehested, Catalysis Today 111 (2006) 103-110.

[5] H. Bengaard, J.K. Nørskov, J. Sehested, B.S. Clausen, L.P. Nielsen, A.M. Molenbroek, J.R. Rostrup-Nielsen, Journal of Catalysis 209 (2002) 365-384.

[6] V.C.H. Kroll, H.M. Swaan, C. Mirodatos, Journal of Catalysis 161 (1996) 409-422.

[7] S. Wang, G.Q. Lu, G.J. Millar, Energy & Fuels 10 (1996) 896-904.

[8] F. Besenbacher, I. Chorkendorff, B. Clausen, B. Hammer, A. Molenbroek, J.K. Nørskov, I. Stensgaard, Science 279 (1998) 1913-1915.

[9] M. García-Diéguez, E. Finocchio, M.Á. Larrubia, L.J. Alemany, G. Busca, Journal of Catalysis 274 (2010) 11-20.

[10] M. García-Diéguez, I.S. Pieta, M.C. Herrera, M.A. Larrubia, L.J. Alemany, Applied Catalysis A: General 377 (2010) 191-199.

[11] B. Pawelec, S. Damyanova, K. Arishtirova, J.L.G. Fierro, L. Petrov, Applied Catalysis A: General 323 (2007) 188-201.

[12] W. Yu, M.D. Porosoff, J.G. Chen, Chemical Reviews 112 (2012) 5780-5817.

[13] S.R. de Miguel, I.M.J. Vilella, S.P. Maina, D.S. José-Alonso, M.C. Román-Martínez, M.J. Illán-Gómez, Applied Catalysis A: General 435-436 (2012) 10-18.

[14] G. Jones, J.G. Jakobsen, S.S. Shim, J. Kleis, M.P. Andersson, J. Rossmeisl, F. Abild-Pedersen, T. Bligaard, S. Helveg, B. Hinnemann, J.R. Rostrup-Nielsen, I. Chorkendorff, J. Sehested, J.K. Nørskov, Journal of Catalysis 259 (2008) 147-160.

[15] F. Abild-Pedersen, J.K. Nørskov, J.R. Rostrup-Nielsen, J. Sehested, S. Helveg, Physical Review B 73 (2006) 115419.

[16] T. Aaltonen, M. Ritala, T. Sajavaara, J. Keinonen, M. Leskela¨, Chemistry of Materials 15 (2003) 1924-1928.

[17] Y. Zhou, D.M. King, X. Liang, J. Li, A.W. Weimer, Applied Catalysis B: Environmental 101 (2010) 54-60.

[18] J. Li, X. Liang, D.M. King, Y.-B. Jiang, A.W. Weimer, Applied Catalysis B: Environmental 97 (2010) 220-226.

[19] W. Setthapun, W.D. Williams, S.M. Kim, H. Feng, J.W. Elam, F.A. Rabuffetti, K.R. Poeppelmeier, P.C. Stair, E.A. Stach, F.H. Ribeiro, J.T. Miller, C.L. Marshall, The Journal of Physical Chemistry C 114 (2010) 9758-9771.

[20] W. Kessels, H. Knoops, S. Dielissen, A. Mackus, M. van de Sanden, Applied Physics Letters 95 (2009) 013114.

[21] X. Liang, L. Lyon, Y.-B. Jiang, A. Weimer, Journal of Nanoparticle Research 14 (2012) 1-12.

[22] S.T. Christensen, H. Feng, J.L. Libera, N. Guo, J.T. Miller, P.C. Stair, J.W. Elam, Nano Letters 10 (2010) 3047-3051.

[23] Y. Lei, B. Liu, J. Lu, R.J. Lobo-Lapidus, T. Wu, H. Feng, X. Xia, A.U. Mane, J.A. Libera, J.P. Greeley, J.T. Miller, J.W. Elam, Chemistry of Materials 24 (2012) 3525-3533.

[24] A.J.M. Mackus, N. Leick, L. Baker, W.M.M. Kessels, Chemistry of Materials 24 (2012) 1752-1761.

[25] T.D. Gould, A.M. Lubers, B.T. Neltner, J.V. Carrier, A.W. Weimer, J.L. Falconer, J. Will Medlin, Journal of Catalysis 303 (2013) 9-15.

[26] D.M. King, J.A. Spencer Ii, X. Liang, L.F. Hakim, A.W. Weimer, Surface and Coatings Technology 201 (2007) 9163-9171.

[27] D.A. Shirley, Physical Review B 5 (1972) 4709-4714.

[28] D. Baudouin, U. Rodemerck, F. Krumeich, A.d. Mallmann, K.C. Szeto, H. Ménardd, L. Veyre, J.-P. Candy, P.B. Webb, C. Thieuleux, C. Copéreta, Journal of Catalysis 297 (2013) 27-34.

[29] A. Olafsen, C. Daniel, Y. Schuurman, L. Råberg, U. Olsbye, C. Mirodatos, Catalysis Today 115 (2006) 179-185.

[30] G. Kresse, J.R. Furthmueller, Computational Materials Science 6 (1996) 15-50.

[31] G. Kresse, J.R. Hafner, Physical Review B 47 (1993) 558-561.

[32] P.E. Blöchl, Physical Review B 50 (1994) 17953-17979.

[33] G. Kresse, D. Joubert, Physical Review B 59 (1999) 1758-1775.

[34] M.M. Montemore, J.W. Medlin, The Journal of Physical Chemistry C 117 (2013) 20078-20088.

[35] N. İnoğlu, J.R. Kitchin, Journal of Catalysis 261 (2009) 188-194.

[36] D. Sun, Y. Zhao, H. Su, W. Li, Chinese Journal of Catalysis 34 (2013) 1434-1442.

[37] A. Olafsen, Ã. Slagtern, I.M. Dahl, U. Olsbye, Y. Schuurman, C. Mirodatos, Journal of Catalysis 229 (2005) 163-175.

[38] D. Baudouin, K.C. Szeto, P. Laurent, A. De Mallmann, B. Fenet, L. Veyre, U. Rodemerck, C. Copéret, C. Thieuleux, Journal of the American Chemical Society 134 (2012) 20624-20627.

[39] C.H. Bartholomew, Applied Catalysis A: General 107 (1993) 1-57.

[40] J. Sehested, Journal of Catalysis 217 (2003) 417-426.

[41] R.T.K. Baker, Carbon 27 (1989) 315-323.

[42] E.F. Kukovitsky, S.G. L'Vov, N.A. Sainov, V.A. Shustov, L.A. Chernozatonskii, Chemical Physics Letters 355 (2002) 497-503.

[43] A. Tanksale, J.N. Beltramini, J.A. Dumesic, G.Q. Lu, Journal of Catalysis 258 (2008) 366-377.

[44] A. Jentys, B.J. McHugh, G.L. Haller, J.A. Lercher, The Journal of Physical Chemistry 96 (1992) 1324-1328.

[45] S.A. Tupy, A.M. Karim, C. Bagia, W. Deng, Y. Huang, D.G. Vlachos, J.G. Chen, ACS Catalysis 2 (2012) 2290-2296.

[46] L.M. Aparicio, Journal of Catalysis 165 (1997) 262-274.

[47] A.K. Avetisov, J.R. Rostrup-Nielsen, V.L. Kuchaev, J.H. Bak Hansen, A.G. Zyskin, E.N. Shapatina, Journal of Molecular Catalysis A: Chemical 315 (2010) 155-162.

[48] W. Erley, H. Wagner, Surface Science 74 (1978) 333-341.

[49] J.R. Kitchin, N.A. Khan, M.A. Barteau, J.G. Chen, B. Yakshinskiy, T.E. Madey, Surface Science 544 (2003) 295-308.

[50] R. Mu, Q. Fu, H. Liu, D. Tan, R. Zhai, X. Bao, Applied Surface Science 255 (2009) 7296-7301.

[51] F. Pompeo, N.N. Nichio, M.M. Souza, D.V. Cesar, O.A. Ferretti, M. Schmal, Applied Catalysis A: General 316 (2007) 175-183.

[52] E. Nikolla, A. Holewinski, J. Schwank, S. Linic, Journal of the American Chemical Society 128 (2006) 11354-11355.

Graphical Abstract artwork:

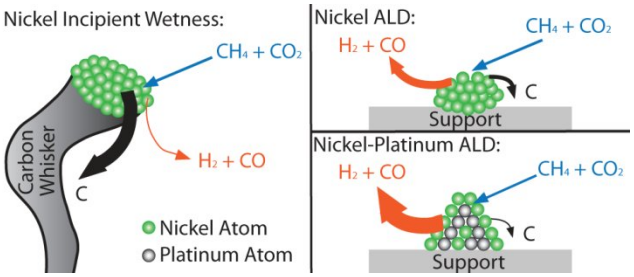

Figure Captions:

Figure 1. A) DRM reforming rates as a function of time for Ni IW and Ni ALD catalysts at 600°C. Both porous and nanosphere Al_2O_3 supports were used for the Ni ALD catalysts. B) TEM image showing carbon whiskers on the Ni IW catalyst supported on porous Al_2O_3 after 36 h on-stream. C) TEM image of Ni ALD catalysts on nonporous Al_2O_3 spheres after 72 h of DRM at 600°C.

Table 1. Catalyst composition and chemisorption results

Figure 2. Hydrogen uptake of Ni, Pt, and NiPt catalysts obtained by temperature-programed reduction.

Figure 3. Adsorbate dependent surface termination of Ni-Pt bimetallic surfaces, where a positive value indicates that Pt/Ni/NiPt is more favorable and a negative value indicates that Ni/Pt/NiPt is more favorable. Insets show metallic structures that were used for the DFT calculations. The values on the y-axis represent eV/unit cell area.

Figure 4. Phase diagram for NiPt bimetallic surfaces as a function of the CO and CO_2 chemical potentials. The "X" denotes representative chemical potentials of the adsorbates during the experiments in this work assuming atmospheric total pressure.

Figure 5. Carbon monoxide temperature-programmed desorption of Ni-Pt ALD catalysts before and after reaction.

Figure 6. *In-situ* XPS spectra for (a) a Ni-Pt crystalline surface (a) exposed to O_2 (4.3 x 10^{-5} Pa pressure) for 30 min at 227 °C; (b)) subsequently annealed to 250 °C in an equimolar mixture of CO_2 and CH_4 (130 Torr total pressure); (c) subsequently annealed to 400 °C in H_2 (4.3 x 10^{-5} Pa pressure); and (d) subsequently annealed to 300 °C in an equimolar mixture of CO_2 and CH_4 (130 Torr total pressure). See the main text for the full details of the experimental sequence.

Figure 7. Steady-state rates of dry reforming of methane at 600°C normalized per gram of metal. The three bimetallic catalysts had Pt added to the two Ni catalysts shown on the left. Error bars represent standard deviation.

Table 2. Comparison of DRM rates for Ni and NiPt catalysts

Figure 8. A) Carbon and oxygen adsorption energies of different metal surfaces. B) CO formation and CH_4 dissociation energies of different metal surfaces.

Figure 9. (A) Bimetallic NiPt ALD catalyst particles after 32 h of reaction at 600°C indicate varying particle sizes with minimal carbon whisker deposition. Metal particles (dark <20 nm) were supported on spherical alumina supports. (B) NiPt catalyst prepared by IW after 42 h of reaction show growth of carbon whiskers.

Table 3. Barriers to Atomic Carbon Diffusion.